Local spin dynamics with the electron electric dipole moment

Masahiro Fukuda, Kota Soga, Masato Senami, and Akitomo Tachibana*
Department of Micro Engineering, Kyoto University, Kyoto 615-8540, Japan
(Received 14 October 2015; published 25 January 2016)

The local spin dynamics of the electron is studied from the viewpoint of the electric dipole moment (EDM) of the electron in the framework of the quantum field theory. The improvements of the computational accuracy of the effective electric field ($\mathcal{E}_{\rm eff}$) for the EDM and the understanding of spin precession are important for the experimental determination of the upper bound of the EDM. Calculations of $\mathcal{E}_{\rm eff}$ in YbF ($^2\Sigma_{1/2}$), BaF ($^2\Sigma_{1/2}$), ThO ($^3\Delta_1$), and HF^+ ($^2\Pi_{1/2}$) are performed on the basis of the restricted active space configuration interaction approach by using the four-component relativistic electronic structure calculation. The spin precession is also discussed from the viewpoint of local spin torque dynamics. We show that a contribution to the torque density for the spin is brought into by the EDM. Distributions of the local spin angular momentum density and torque densities induced by external fields in the above molecules are calculated and a property related with large $\mathcal{E}_{\rm eff}$ is discussed.

DOI: 10.1103/PhysRevA.93.012518

I. INTRODUCTION

The permanent electric dipole moment (EDM) of the electron is a significant key to reveal a violation of the time-reversal ($\mathcal{T}$) symmetry. With the $\mathcal{CPT}$ invariance, this means the violation of the product of the associated charge ($\mathcal{C}$) and the spatial parity ($\mathcal{P}$), and this $\mathcal{CP}$ violation may be a hint of the mystery of the dominance of matter over antimatter in our universe. The value of the electron EDM (d_e) predicted by the standard model of particle physics ($d_e \sim 10^{-40}$ e cm) is too small to be observed by present experiments. However, some extensions of the standard model, such as low-energy supersymmetric models [1], predict much larger d_e, for example $d_e \sim 10^{-27}$–10^{-29} e cm in a supersymmetric model [2]. Therefore, the existence of a nonzero electron EDM provides the evidence of the $\mathcal{T}$ violation and judges some extension theories. In the present experiments, the upper bound of the EDM derived by using ThO and YbF molecules is reported as $d_e < 8.7 \times 10^{-29}$ [3] and $d_e < 1.05 \times 10^{-27}$ e cm [4], respectively. Hence these constraints are already in ranges predicted by supersymmetric models and experiments in the near future will find or rule out extension models of the standard model.

Experiments for searching the EDM rely on observations of spin precession induced by an electric field. Hence a larger electric field is more efficient to determine the upper bound of the electron EDM. Recently, heavy polar diatomic molecules are chosen for experimental searches for the electron EDM, since an internal electric field in polar molecules is much larger than an external electric field in the laboratory ($\sim$100 kV/cm). Actually, the effective electric field is reported to be 1–100 GV/cm for many polar molecules, for example YbF, BaF, and ThO by numerical computations [5–8]. In this work, we focus on the value of the effective electric field by using these diatomic molecules. In order to determine the upper bound of d_e, both the interaction energy of the EDM ($E_{\rm EDM}$) and the effective electric field ($\mathcal{E}_{\rm eff} = E_{\rm EDM}/d_e$) are needed. The former can be experimentally measured by observations of spin precession, while the latter needs to be predicted by using *ab initio* calculations based on the relativistic quantum theory because relativistic effects and correlation effects are essentially important for the computation of heavy atoms. For the relativistic effects, the four-component Dirac equation should be solved to include relativistic interactions such as the spin-orbit interaction. For the correlation effects, post Hartree-Fock computations, such as configuration interaction (CI), are required. These two treatments result in a very large computational cost to calculate the effective electric field. Although some works have already been reported on the values of the effective electric field in diatomic molecules [5–8] by *ab initio* calculations with some approximations, the improvement of the precision of $\mathcal{E}_{\rm eff}$ is important for the accurate estimate of the experimental bound of the EDM. Another key point is a treatment of spin precession. The quantum mechanical approaches for spin dynamics are widely used; however, these approaches cannot explain local spin dynamics since a physical quantity in the quantum mechanics is defined by the inner product, which is derived by the integration over the whole region. In the quantum field theory, local distributions of physical quantities such as the spin angular momentum density and torque density for the spin can be predicted. The equation of motion of the spin based on the quantum field theory was proposed in Ref. [9], and our group has already discussed the local contribution of the spin torque by using numerical calculations particularly for a spin stationary state of the diatomic system of alkali atoms [10], transition element atoms [11], and allene-type molecules with chiral and achiral structures [12].

In this work, we investigate the relation between the electron EDM and the spin in the quantum field theory. The relation between the interaction energy of the electron EDM and the spin precession is explained by an approximate description of time evolution originated from the existence of the EDM. Using two approximation methods to evaluate the effective electric field, we calculate the effective electric field in YbF, BaF, ThO, and HF^+ molecules by *ab initio* calculations based on the relativistic quantum mechanics. We reconsider the spin precession from the viewpoint of the local spin torque dynamics described by the equation of motion of the spin

*akitomo@scl.kyoto-u.ac.jp

angular momentum density in the quantum field theory. The equation of motion of the spin is modified by the nonzero electron EDM, and then the torque density contribution is revealed. After a discussion of the calculation results of the effective electric field, the local distribution of physical quantities, the spin angular momentum density, and the EDM torque density induced by external fields are calculated and discussed. The reason that the effective electric field in YbF is much larger than that in HF^+ is discussed from the viewpoint of the local physical quantities. This local distribution analysis indicates that even light atomic molecules could have the large effective electric field.

II. THEORY

A. Hamiltonian density with EDM

The Dirac Lagrangian density for the electron is written as

$$\hat{\mathcal{L}}_e = c\hat{\bar{\psi}}(i\hbar\gamma^\mu \hat{D}_{e\mu} - m_e c)\hat{\psi}, \tag{1}$$

where $\hat{\psi}$ denotes the Dirac spinor of the electron, $\hat{\bar{\psi}} = \hat{\psi}^\dagger\gamma^0$, γ^μ are gamma matrices, m_e is the electron mass, and c is the speed of light in vacuum. Here, Greek indices run over 0 to 3. We adopt the Einstein summation convention. The gauge covariant derivative is written as $\hat{D}_{e\mu} = \partial_\mu + i\frac{Z_e e}{\hbar c}\hat{A}_\mu$, where $\hat{A}_\mu$ is the gauge field, e is the electron charge ($e > 0$), and $Z_e = -1$. By using the Euler-Lagrange equation, the equation of motion is given as

$$i\hbar c\gamma^0\gamma^\mu \hat{D}_{e\mu}\hat{\psi} - m_e c^2\gamma^0\hat{\psi} = 0. \tag{2}$$

The Hamiltonian density is derived by the ordinary Legendre transformation,

$$\hat{\mathcal{H}}_e(x) = c\hat{\bar{\psi}}(-i\hbar\gamma^k \cdot \hat{D}_{ek} + m_e c)\hat{\psi} + Z_e e\hat{A}_0\hat{\psi}^\dagger\hat{\psi}, \tag{3}$$

where Latin indices run over 1 to 3. To describe the interaction of the relativistic electron EDM, we employ the gauge- and Lorentz-invariant effective Lagrangian density for the electron EDM,

$$\hat{\mathcal{L}}_{\rm EDM} = -d_e\frac{i}{2}\hat{\bar{\psi}}\sigma^{\mu\nu}\gamma_5\hat{F}_{\mu\nu}\hat{\psi}, \tag{4}$$

where d_e is the electron EDM, $\sigma^{\mu\nu} = \frac{i}{2}[\gamma^\mu,\gamma^\nu]$, $\gamma_5 = i\gamma^0\gamma^1\gamma^2\gamma^3$, and the electromagnetic field strength tensor is $\hat{F}_{\mu\nu} = \partial_\mu\hat{A}_\nu - \partial_\nu\hat{A}_\mu$. This additional term in the Lagrangian extends the Dirac equation [Eq. (2)] as follows:

$$i\hbar c\gamma^0\gamma^\mu \hat{D}_{e\mu}\hat{\psi} - m_e c^2\gamma^0\hat{\psi} - d_e\frac{i}{2}\gamma^0\sigma^{\mu\nu}\gamma_5\hat{F}_{\mu\nu}\hat{\psi} = 0. \tag{5}$$

The EDM Lagrangian density yields the EDM Hamiltonian density,

$$\hat{\mathcal{H}}_{\rm EDM}(x) = d_e\frac{i}{2}\hat{\bar{\psi}}\sigma^{\mu\nu}\gamma_5\hat{F}_{\mu\nu}\hat{\psi} \tag{6}$$

$$= -d_e(\hat{\bar{\psi}}\vec{\Sigma}\cdot\hat{\vec{E}}\hat{\psi} + i\hat{\bar{\psi}}\gamma^0\vec{\gamma}\cdot\hat{\vec{B}}\hat{\psi}), \tag{7}$$

where $\hat{\vec{E}}$ and $\hat{\vec{B}}$ are the electric and magnetic fields, respectively, and $\vec{\Sigma}$ is the 4×4 Pauli matrix.

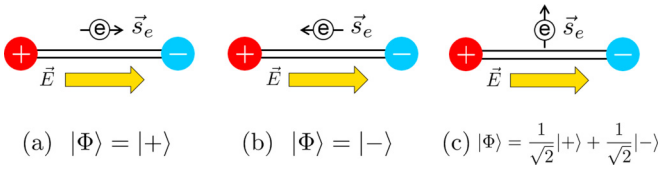

FIG. 1. Schematic pictures of ket states.

B. Spin precession with EDM

Next, we describe a relation between the interaction energy of the EDM and spin precession. At first, neglecting the vector potential term in Eq. (3), we begin with the Dirac-Coulomb Hamiltonian density,

$$\hat{\mathcal{H}}_{\rm DC} = c\hat{\bar{\psi}}(-i\hbar\gamma^k\partial_k + m_e c)\hat{\psi} + Z_e e\hat{A}_0\hat{\psi}^\dagger\hat{\psi}, \tag{8}$$

for the system Hamiltonian. Namely, we treat other contributions, i.e., the effect of the internal vector potential and the EDM interaction, in a perturbative manner. Then, we assume that two time-independent degenerate state vectors, $|+\rangle \equiv \hat{c}_+^\dagger(t_0)|0\rangle$ and $|-\rangle \equiv \hat{c}_-^\dagger(t_0)|0\rangle$ (see Fig. 1), are the Heisenberg ground state of the system satisfying

$$\int \langle\pm| : \hat{\mathcal{H}}_{\rm DC}(\vec{r},t = t_0) : |\pm\rangle d^3\vec{r} = E_0, \tag{9}$$

$$\int \langle\pm| : \hat{J}_{ez}(\vec{r},t = t_0) : |\pm\rangle d^3\vec{r} = \pm|\Omega|, \tag{10}$$

where $\hat{J}_{ez}(x)$ is the total angular momentum density. Here, we represent normal ordering with colons. By the interaction of the EDM, these degenerate states are split into two energy levels,

$$\int \langle\pm| : \hat{\mathcal{H}}_{\rm DC+EDM}(\vec{r},t = t_0) : |\pm\rangle d^3\vec{r} = E_0 \pm E_{\rm EDM}, \tag{11}$$

where $\hat{\mathcal{H}}_{\rm DC+EDM} = \hat{\mathcal{H}}_{\rm DC} + \hat{\mathcal{H}}_{\rm EDM}$. Suppose the Hamiltonian density does not depend on the time; then the electron field can be expanded approximately as the following equation:

$$\hat{\psi}(x) = \sum_{\alpha=\pm}\hat{c}_\alpha(t)\phi_\alpha(\vec{r}),\ \ \hat{c}_\alpha(t) = e^{-i\omega_\alpha(t-t_0)}\hat{c}_\alpha(t_0), \tag{12}$$

where $\omega_\pm = (E_0 \pm E_{\rm EDM})/\hbar$. In this two-state system, a general Heisenberg state vector can be written as $|\Phi\rangle = \lambda_+|+\rangle + \lambda_-|-\rangle$, where λ_α is the normalization constant which obeys $|\lambda_+|^2 + |\lambda_-|^2 = 1$. The arbitrary operator of physical quantities $\hat{\vec{\mathcal{O}}}(x)$ such as the total angular momentum density can be written as

$$\hat{\vec{\mathcal{O}}}(x) = \sum_{\alpha,\beta=\pm}\vec{\mathcal{O}}_{\alpha\beta}(\vec{r})\hat{c}_\alpha^\dagger(t)\hat{c}_\beta(t)$$

$$= \sum_{\alpha,\beta=\pm}\vec{\mathcal{O}}_{\alpha\beta}(\vec{r})\hat{c}_\alpha^\dagger(t_0)\hat{c}_\beta(t_0)e^{+i(\omega_\alpha-\omega_\beta)(t-t_0)}. \tag{13}$$

Therefore, the time evolution of the expectation value $\langle\Phi| : \hat{\vec{\mathcal{O}}}(x) : |\Phi\rangle$ depends on the $|\omega_+ - \omega_-| = 2E_{\rm EDM}/\hbar$ approximately. This is why the interaction energy of the EDM can be determined by the observation of the spin precession.

C. The effective electric field for the electron EDM

While the observation of spin precession enables us to determine the interaction energy of the electron EDM $E_{\rm EDM}$, we must still evaluate the effective electric field for the electron EDM $\mathcal{E}_{\rm eff} = E_{\rm EDM}/d_e$ to determine the value of d_e. In heavy polar diatomic molecules, which were recently chosen for experimental searches for the electron EDM, it is known that the magnetic term of the interaction energy of the electron EDM, $E^B_{\rm EDM}$ [contribution from the second term of Eq. (7)], is much smaller than the electric term, $E^E_{\rm EDM}$ [contribution from the first term of Eq. (7)]. Hence, we can write $\mathcal{E}_{\rm eff} \approx E^E_{\rm EDM}/d_e$, and this is represented as the following form:

$$\begin{aligned}\mathcal{E}_{\rm eff} &\approx \frac{1}{d_e}\int \langle\Phi| : \hat{\mathcal{H}}^E_{\rm EDM}(\vec{r}) : |\Phi\rangle d^3\vec{r} \\ &\approx \int \langle\Phi| : -\hat{\vec{\Sigma}}\cdot\hat{\vec{E}}\hat{\psi} : |\Phi\rangle d^3\vec{r} \\ &\approx \int \langle\Phi| : -\hat{\vec{\Sigma}}\cdot(\hat{\vec{E}}^{\rm ele}+\hat{\vec{E}}^{\rm nuc})\hat{\psi} : |\Phi\rangle d^3\vec{r}, \end{aligned} \tag{14}$$

where $\hat{\vec{E}}^{\rm ele}(\vec{r})[\hat{\vec{E}}^{\rm nuc}(\vec{r})]$ is the electric field contributed by electrons [nuclei]. To avoid time-consuming calculations about the first term of Eq. (14), some approximations are used for the internal electric field in a molecule. Two types of approximations are often used. One is the approximation that the internal electric field is replaced only with $\hat{\vec{E}}^{\rm nuc}(\vec{r})$ as follows:

$$\begin{aligned}\mathcal{E}_{\rm eff} &\approx \int \langle\Phi| : -\hat{\psi}^\dagger\left(\gamma^0-1\right)\vec{\Sigma}\cdot\hat{\vec{E}}\hat{\psi} : |\Phi\rangle d^3\vec{r} \\ &\approx \int \langle\Phi| : 2\hat{\psi}_S^\dagger\vec{\sigma}\cdot\hat{\vec{E}}\hat{\psi}_S : |\Phi\rangle d^3\vec{r} \\ &\approx \int \langle\Phi| : 2\hat{\psi}_S^\dagger\vec{\sigma}\cdot\hat{\vec{E}}^{\rm nuc}\hat{\psi}_S : |\Phi\rangle d^3\vec{r}, \end{aligned} \tag{15}$$

where $\hat{\psi}_S$ is the small component of the four-component dirac spinor $\hat{\psi}$. At the first line, we use the Schiff's theorem [13]. The deviation by the approximation in the last line is reported to be within 3% for the computation of the effective electric field in YbF [5]. This is because the small component of the spin angular momentum density is concentrated on the Yb nucleus.

The other approximation is a method which uses the so-called effective one-body EDM operator [14] as follows:

$$\mathcal{E}_{\rm eff} \approx \int \langle\Phi| : \frac{2i\hbar c}{Z_e e}\hat{\psi}^\dagger\gamma^0\gamma_5\Delta\hat{\psi} : |\Phi\rangle d^3\vec{r}, \tag{16}$$

where the equation is satisfied only if $|\Phi\rangle$ is exactly an eigenstate of $\int \mathcal{H}_{\rm DC} d^3\vec{r}$ due to the Schiff's theorem [13].

In later arguments, we discuss the parallel magnetic hyperfine interaction constant defined as

$$A_\parallel = \frac{\mu_K}{I\Omega}\int \langle\Phi| : \left(Z_e e\hat{\vec{\psi}}\frac{\vec{\gamma}\times\vec{r}}{|\vec{r}|^3}\hat{\psi}\right)_z : |\Phi\rangle d^3\vec{r}, \tag{17}$$

where μ_K is the nuclear magnetic dipole moment, I is the nuclear spin quantum number, and Ω is the quantum number of the total electronic angular momentum projection onto the internuclear axis. In addition, the molecular electric dipole moment (DM) is introduced as

$$\vec{\mu} = \int \langle\Phi| : \vec{r}\hat{\rho}(\vec{r}) : |\Phi\rangle d^3\vec{r}, \tag{18}$$

$$\hat{\rho}(\vec{r}) = Z_e e\hat{\psi}^\dagger\hat{\psi} + \sum_{a=1}^{N_A} Z_a e\delta(\vec{r}-\vec{R}_a), \tag{19}$$

where N_A is the number of nuclei, and Z_a and $\vec{R}_a$ are the charge and the position of each nucleus, respectively. The DM as well as $A_\parallel$ is useful to estimate the accuracy of the electronic structure.

D. Local spin torque dynamics with EDM

We reconsider the spin precession from the viewpoint of the local spin torque dynamics. In the quantum field theory without the interaction of the electron EDM, the spin angular momentum density and its time derivative are given by [9,15]

$$\hat{\vec{s}}_e(x) = \hat{\psi}^\dagger(x)\frac{\hbar}{2}\vec{\Sigma}\hat{\psi}(x), \tag{20}$$

$$\frac{\partial}{\partial t}\hat{\vec{s}}_e(x) = \hat{\vec{t}}_e(x) + \hat{\vec{\zeta}}_e(x), \tag{21}$$

where Eq. (21) is derived by using Eq. (2). The first term of the right-hand side of Eq. (21) is called the spin torque density, which gives, by the integration over the whole region, the spin torque in the Heisenberg equation of the spin in the relativistic quantum mechanics [16]. The spin torque density can be written as

$$\hat{t}^i_e(x) = \hat{t}^i_{eN}(x) + \hat{t}^i_{eA}(x), \tag{22}$$

$$\hat{t}^i_{eN}(x) = -\frac{i\hbar c}{2}\epsilon_{ijk}\hat{\psi}^\dagger(x)\gamma^0\gamma^k\partial_j\hat{\psi}(x) + \text{H.c.}, \tag{23}$$

$$\hat{t}^i_{eA}(x) = -Z_e e\epsilon_{ijk}\hat{\psi}^\dagger(x)\gamma^0\gamma^k\hat{A}^j(x)\hat{\psi}(x), \tag{24}$$

where ϵ_{ijk} is the Levi-Civita tensor. We note that $\hat{\vec{t}}_{eA}$ is the torque by the contribution proportional to $\hat{\vec{A}}$. The second term of the right-hand side of Eq. (21), which is named the zeta force density, is given as

$$\hat{\zeta}^i_e(x) = -\partial_i\hat{\phi}_5(x), \tag{25}$$

$$\hat{\phi}_5(x) = \frac{\hbar c}{2}\hat{\psi}^\dagger(x)\gamma_5\hat{\psi}(x). \tag{26}$$

The zeta force density $\hat{\vec{\zeta}}_e$ is represented as the gradient of the zeta potential $\hat{\phi}_5$, which can be rewritten as $\hat{\phi}_5 = \frac{\hbar c}{2}(\hat{\psi}^\dagger_R\hat{\psi}_R - \hat{\psi}^\dagger_L\hat{\psi}_L)$ by using the right-handed and left-handed spinors: $\hat{\psi}_R = [(1+\gamma_5)/2]\hat{\psi}$ and $\hat{\psi}_L = [(1-\gamma_5)/2]\hat{\psi}$. The zeta force density integrated over the whole region is zero, as seen from Eq. (25). Hence when we consider the equation of motion of the spin after the integration, the local contribution of the zeta force density is lost and Eq. (21) can be identified with the ordinary Heisenberg equation of the spin in the relativistic quantum mechanics [16]. Note that Eq. (21) is known to be derived naturally by the "quantum spin vorticity principle" [17–21].

The contribution of the electron EDM to the torque for the spin is considered. The EDM Lagrangian [Eq. (4)] gives the

TABLE I. Bond length for each molecule.

Species (state)	Bond length (Å)
YbF ($^2\Sigma_{1/2}$)	2.073
ThO ($^3\Delta_1$)	1.840
BaF ($^2\Sigma_{1/2}$)	2.253 (DZ)
	2.189 (TZ)
	2.182 (QZ)
HF^+ ($^2\Pi_{1/2}$)	0.991 (DZ)
	0.987 (TZ)
	0.986 (QZ)

TABLE II. Nuclear magnetic dipole moment for each atom in Ref. [25]. The uncertainty in the experimental result is given in parentheses.

Species	I	μ_K[a] (nm)
$^{171}_{70}$Yb	1/2	0.4937
$^{229}_{90}$Th	5/2	0.46(4)
$^{137}_{56}$Ba	3/2	0.9374

[a]μ_K is the K's nuclear magnetic dipole moment in units of the nuclear magneton μ_N (nm).

additional local spin torque density $\hat{\hat{t}}_{\rm EDM}(x)$,

$$\hat{\hat{t}}_{\rm EDM}(x) = \hat{\hat{t}}^E_{\rm EDM}(x) + \hat{\hat{t}}^B_{\rm EDM}(x), \tag{27}$$

$$\hat{\hat{t}}^E_{\rm EDM}(x) = d_e \hat{\hat{\psi}}(x)[\vec{\Sigma} \times \hat{\hat{E}}(x)]\hat{\psi}(x), \tag{28}$$

$$\hat{\hat{t}}^B_{\rm EDM}(x) = d_e i \hat{\hat{\psi}}(x)\gamma^0[\vec{\gamma} \times \hat{\hat{B}}(x)]\hat{\psi}(x), \tag{29}$$

where we separate the EDM torque density $\hat{\hat{t}}_{\rm EDM}$ into the electric term $\hat{\hat{t}}^E_{\rm EDM}$ and the magnetic term $\hat{\hat{t}}^B_{\rm EDM}$. We note that the EDM torque has a component perpendicular to both the electric and magnetic fields. Finally, the equation of motion of the spin angular momentum density with the contribution of the electron EDM is summarized as

$$\frac{\partial}{\partial t}\hat{\hat{s}}_e(x) = \hat{\hat{t}}_e(x) + \hat{\hat{\zeta}}_e(x) + \hat{\hat{t}}_{\rm EDM}(x). \tag{30}$$

For example, in recent experiments for the electron EDM, using heavy polar diatomic molecules, the spin precession of the state $|\Phi\rangle = (|+\rangle + |-\rangle)/\sqrt{2}$ (see Fig. 1) is observed. The torque accelerating spin by the EDM effective electric field corresponds to $\int \langle\Phi|\hat{\hat{t}}_{\rm EDM}(x)|\Phi\rangle d^3\vec{r}$. However, our Eq. (30) can explain even local distributions of the physical quantities in a molecule. If one could estimate the spin angular momentum density and the local torque densities in a local region, it would present a different way to observe the electron EDM. In a later section, we calculate the local distribution of such quantities as a demonstration.

III. COMPUTATIONAL DETAILS

We calculate the effective electric fields for the purpose of checking the accuracy of the electronic state by comparing the other groups' results of the effective electric field in order to prepare the electronic states for calculations of the local physical quantities. All of the effective electric fields are consistently calculated at the configuration interaction with all single and double excitations (CISD) level to serve as useful references. We calculate the effective electric fields in YbF ($^2\Sigma_{1/2}$), BaF ($^2\Sigma_{1/2}$), and ThO ($^3\Delta_1$) under the two types of approximations, Eqs. (15) and (16). In order to investigate the origin of large effective electric fields, we also calculate the effective electric field in HF^+ ($^2\Pi_{1/2}$), which also has a large molecular electric dipole moment. We use four-component wave functions of these molecules in the relativistic quantum mechanics as a substitution of those in the quantum field theory. The four-component wave functions are derived by using the DIRAC13 program package [22]. We use the uncontracted Dyall's four-component double zeta (DZ), triple zeta (TZ), and quadruple zeta (QZ) basis sets, which have correlating functions for all shells [23]. After Dirac-Hartree-Fock computations with the Dirac-Coulomb Hamiltonian, CI computations are performed in the restricted active space

TABLE III. Effective electric field in YbF. The uncertainty in the experimental result is given in parentheses.

YbF($^2\Sigma_{1/2}$) Method/Basis	Active orbitals	Vert. orb. cutoff (Hartree)	$\mathcal{E}^{\rm ob}_{\rm eff}$ ($\frac{\rm GV}{\rm cm}$)	$\mathcal{E}^{\rm nuc}_{\rm eff}$ ($\frac{\rm GV}{\rm cm}$)	$\lvert A^{\rm Yb}_{\parallel}\rvert$ (MHz)	DM (D)
31e-CISD/DZ	25–80	1.82	21.0	21.7	6207	3.49
31e-CISD/TZ	25–80	0.92	19.7	20.1	5674	3.59
31e-CISD/QZ	25–80	0.60	19.8	20.2	5727	3.59
31e-CISD/QZ	25–109	1.30	20.8	21.2	5992	3.45
31e-CISD/QZ	25–127	2.00	20.3	20.7	5885	3.38
79e-CISD/QZ	1–109	1.30	20.8	21.2	6002	3.44
Experiment					7822(5)[a]	3.91(4)[b]
GRECP/RASSCF/EO[c]				24.9	7842	
31e-RASCI[d]				24.06		
79e-CCSD/QZ[e]			23.1			3.60

[a]Reference [27].
[b]Reference [28].
[c]Reference [29].
[d]Reference [30].
[e]Reference [6].

TABLE IV. Effective electric field in BaF. The uncertainty in the experimental result is given in parentheses.

BaF($^2\Sigma_{1/2}$) Method/Basis	Active orbitals	Vert. orb. cutoff (Hartree)	$\mathcal{E}_{\rm eff}^{\rm ob}$ ($\frac{\rm GV}{\rm cm}$)	$\mathcal{E}_{\rm eff}^{\rm nuc}$ ($\frac{\rm GV}{\rm cm}$)	$\lvert A_\parallel^{\rm Ba}\rvert$ (MHz)	DM (D)
17e-CISD/DZ	25–92	8.00	4.62	4.87	1647	3.08
17e-CISD/TZ	25–92	2.20	4.58	4.67	1580	2.20
17e-CISD/QZ	25–92	0.80	4.51	4.58	1552	2.36
65e-CISD/DZ	1–92	8.00	4.32	4.56	1589	3.11
Experiment					2453(9)[a]	3.1702(15)[b]
RASSCF/EO[c]			7.51		2224	
17e-RASCI[d]				7.28		3.203

[a]Reference [31].
[b]Reference [32].
[c]Reference [33].
[d]Reference [7].

(RAS) method by using the DIRRCI module. We carry out various CISD calculations to investigate the effect of a basis set and the importance of core correlation effects. We refer to the name of CI wave-function models as ne-CISD or ne-MR$_K$-CISD, where n represents the number of active electrons. Models of ne-MR$_K$-CISD are used only for calculation of the ThO molecule, and MR is the multireference CI. The reference states are generated by average-of-configuration open-shell calculations for averaging with two electrons in the Th($7s$,$6d\delta$) Kramers pairs. The subscript K represents the number of active valence spinor spaces. When $K = 3$, only the Th($7s$,$6d\delta$) spinors are used in the RAS2 space. In another case, $K = 10$, the Th($7s$,$6d$,$7p$,$8s$) spinors are used in the RAS2 space. For YbF and ThO, we performed only a single geometry calculation with the bond length shown in Table I, whose values are reported in Refs. [24] and [8] for YbF and ThO, respectively. For BaF and HF^+, their bond lengths are determined by geometrical optimization computations at the Hartree-Fock level.

The nuclear-spin quantum numbers I and the nuclear magnetic dipole moments μ_K used in the calculations of the nuclear magnetic hyperfine coupling constant are listed in Table II. Although the experimental value $\mu_{\rm Th}$ does not have even two significant digits, we adopt the center value $\mu_{\rm Th} = 0.46$ as the face value for calculations of $|A_\parallel^{\rm Th}|$, by neglecting its accuracy. In addition, we investigate the distributions of the electron density and the local spin angular momentum density in these molecules to investigate the origin of large effective electric fields.

We also investigate the distributions of the local spin torque density and the local EDM torque density of YbF as a demonstration. For the demonstration, we use the normalized external electric field and magnetic field to make the demonstration simple. Namely, we consider a situation that the external static electric field $\vec{E}_{\rm ext} = (1,0,0)$ and magnetic field $\vec{B}_{\rm ext} = (1,0,0)$ (in atomic units) are applied at $t = 0$ on YbF. Then, the external vector potential is set to $\vec{A}_{\rm ext} = \frac{1}{2}\vec{B}_{\rm ext} \times \vec{r}$. Even if the external fields are multiplied by a constant number, the distribution pattern of the torque density does not change. If we investigate the spin precession used in present EDM experiments, the state $|\Phi\rangle = (|+\rangle + |-\rangle)/\sqrt{2}$ (see Fig. 1) should be used. However, it is hard to calculate the EDM torque term induced by the internal electric field for its state. Therefore, we choose the state $|\Phi\rangle = |-\rangle$, which is the same one used for the calculation of the effective electric field. The electric field induced by the internal particle is not included in our computations of local torque density for this state, since the direction of the integration of the internal electric field over a molecule is the same as that of the spin and the contribution to the EDM torque is considered to be small, as seen from Eq. (28). The computations of the effective electric field and local physical quantities are performed by the QEDynamics program package [26] developed in our group.

TABLE V. Effective electric field in ThO. The uncertainty in the experimental result is given in parentheses.

ThO($^3\Delta_1$) Method/Basis	Active orbitals	Vert. orb. cutoff (Hartree)	$\mathcal{E}_{\rm eff}^{\rm ob}$ ($\frac{\rm GV}{\rm cm}$)	$\mathcal{E}_{\rm eff}^{\rm nuc}$ ($\frac{\rm GV}{\rm cm}$)	$\lvert A_\parallel^{\rm Th}\rvert$ (MHz)	DM (D)
18e-MR$_3$-CISD/DZ	41–109	2.00	68.8	71.1	1154	3.47
18e-MR$_3$-CISD/TZ	41–134	2.00	67.2	69.4	1330	3.53
18e-MR$_3$-CISD/TZ	41–185	2.00	66.5	68.6	1151	3.66
18e-MR$_{10}$-CISD/DZ	41–109	2.00	75.6	78.1	1280	3.86
18e-MR$_{10}$-CISD/TZ	41–134	2.00	71.3	73.6	1156	3.86
Experiment						4.098(3)[a]
18e-MR$_{12}$-CISD/TZ[b]			75.2		1369	
38e-2c-CCSD(T)[c]			81.5		1357	4.23

[a]Reference [34].
[b]Reference [8].
[c]Reference [35].

TABLE VI. Effective electric field in HF^+.

$HF^+(^2\Pi_{1/2})$ Method/Basis	Active orbitals[a]	$\mathcal{E}_{\rm eff}^{\rm ob}$ ($\frac{\rm GV}{\rm cm}$)	$\mathcal{E}_{\rm eff}^{\rm nuc}$ ($\frac{\rm GV}{\rm cm}$)	DM (D)
9e-CISD/DZ	1–42	2.16×10^{-3}	3.65×10^{-3}	2.66
9e-CISD/TZ	1–80	2.53×10^{-3}	3.16×10^{-3}	2.60
9e-CISD/QZ	1–140	2.64×10^{-3}	3.04×10^{-3}	2.59

[a]All of the virtual orbitals are included into the active space.

TABLE VII. Summary of $\mathcal{E}_{\rm eff}$ for each molecule.

Species (state)	Method/Basis	$\mathcal{E}_{\rm eff}^{\rm ob}$ (GV/cm)	$\mathcal{E}_{\rm eff}^{\rm nuc}$ (GV/cm)
YbF ($^2\Sigma_{1/2}$)	79e-CISD/QZ	20.8	21.2
BaF ($^2\Sigma_{1/2}$)	65e-CISD/DZ	4.32	4.56
ThO ($^3\Delta_1$)	18e-MR_{10}-CISD/TZ	71.3	73.6
HF^+ ($^2\Pi_{1/2}$)	9e-CISD/QZ	2.64×10^{-3}	3.04×10^{-3}

IV. RESULTS AND DISCUSSION

The calculation results of the effective electric field with two approximations are shown in Tables III (YbF), IV (BaF), V (ThO), and VI (HF^+). In these tables, $\mathcal{E}_{\rm eff}^{\rm nuc}$ is the approximation using only the nuclear electric field [Eq. (15)] and $\mathcal{E}_{\rm eff}^{\rm ob}$ is the approximation using the effective one-body operator [Eq. (16)]. In our results, the difference between the two approximations is not large and is within a few percents, except for HF^+ which is computed only for a comparison with heavy polar diatomic molecules. This confirms that the large contribution to $\mathcal{E}_{\rm eff}$ arises from electrons near a nucleus, and hence the difference between the two approximations may become large for lighter molecules. For this reason, we also show the parallel magnetic hyperfine interaction constant $A_\parallel$, which is sensitive to the electronic structure near the nucleus.

It is known that a post Hartree-Fock computation is efficient for large basis sets, i.e., triple zeta or larger. Actually, the dependence on basis sets can be clarified from the results of YbF in Table III. The effect of the change from DZ to TZ on calculation results is much larger than that of the change from TZ to QZ. The same feature can be seen in the results of BaF (Table IV). Focusing on the number of active orbitals in Table III, we can find that the number of virtual orbitals included in the CISD calculation is a more influential one than the number of core orbitals in the active space. Although our best result of YbF, 79e-CISD/QZ, is not in sufficient agreement with the experimental data $A_\parallel$, it would be improved by including more virtual orbitals in the CI active space. Nevertheless, the value of the effective electric field is consistent with other theoretical works, though our result is slightly smaller.

Our best result of the dipole moment in BaF (3.11 Debye) is very close to the experimental value (3.1702(15) Debye [32]), whereas the parallel magnetic hyperfine interaction constant (1589 MHz) is far from the experimental value (2453(9) MHz [31]). In addition, our result $\mathcal{E}_{\rm eff}^{\rm nuc} = 4.56$ GV/cm is much smaller than Nayak's result 7.28 GV/cm [7] and Kozlov's result 7.51 GV/cm [33]. The reason seems to be the differences of the number of orbitals in the active space and reference states.

From the results of ThO shown in Table V, the improvement from MR_3-CISD to MR_{10}-CISD brings a notable increase of $\mathcal{E}_{\rm eff}$. Detailed discussions about correlation models of ThO have already been reported in the work of Fleig and Nayak [8]. They mentioned that the addition of σ-type spinors to the active space brings a significant change of the electronic structure of ThO. Our best result $\mathcal{E}_{\rm eff}^{\rm ob} = 71.3$ GV/cm is close enough to the result of Fleig and Nayak, 75.2 GV/cm [8].

As shown in Table VI, the effective electric field in HF^+ is quite small compared to the other molecules, though HF^+ has a large molecular electric dipole moment. The reason is discussed later from a viewpoint of local distribution of physical quantities. Our best results of each molecule are summarized in Table VII. The electronic states of these correlation models are used for the later discussion about local physical quantities.

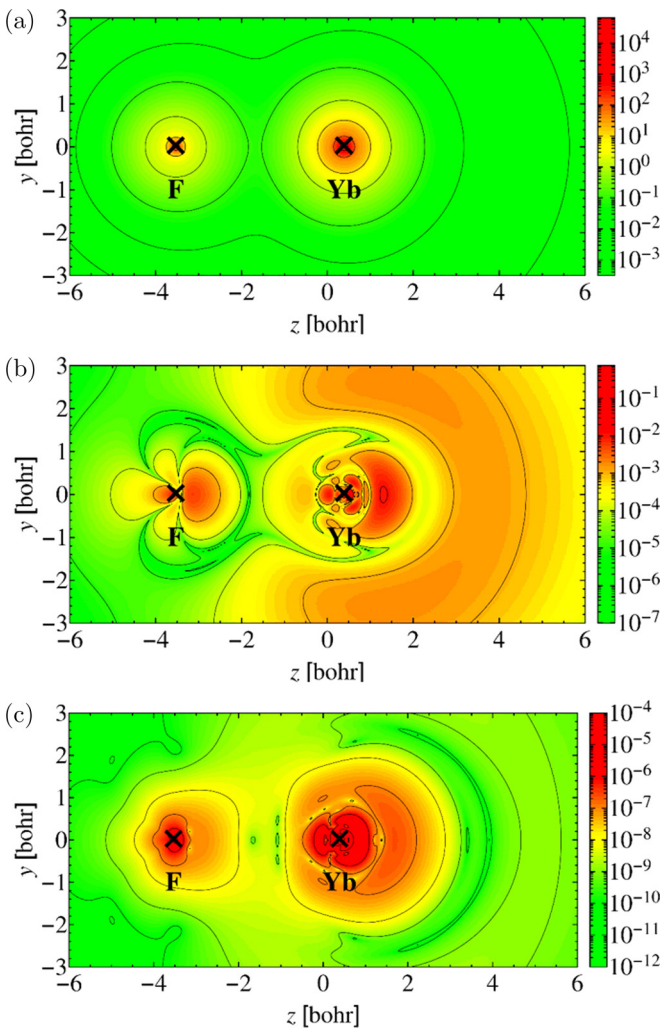

FIG. 2. The distributions of (a) the electron density, (b) the norm of the spin angular momentum density, and (c) the norm of the small component of the spin angular momentum density on a plane including the internuclear axis in YbF. All values are shown in atomic units.

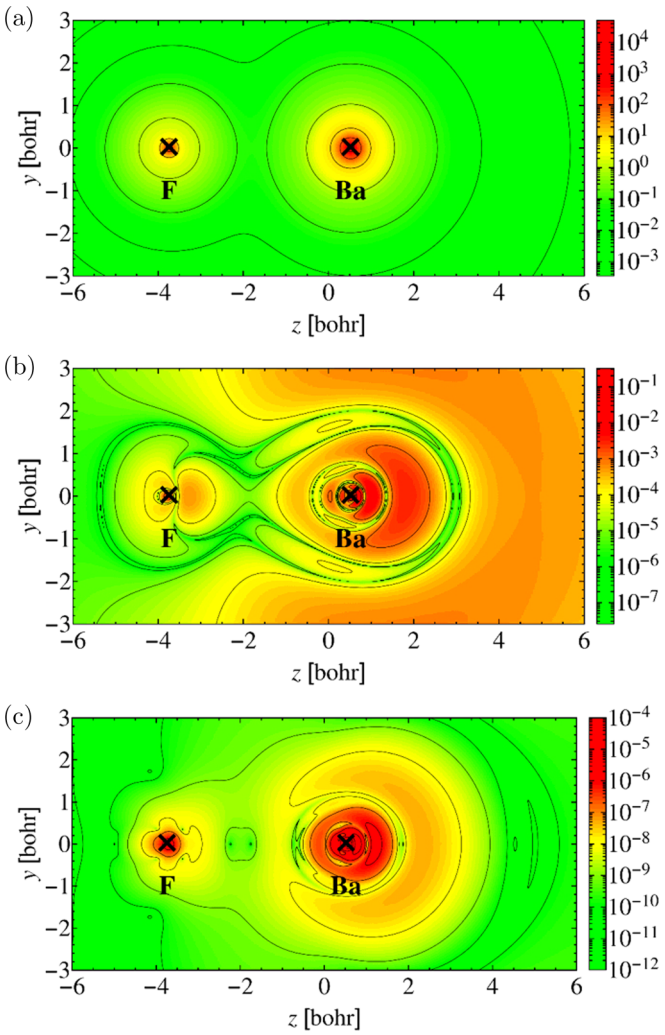

FIG. 3. The distributions of (a) the electron density, (b) the norm of the spin angular momentum density, and (c) the norm of the small component of the spin angular momentum density on a plane including the internuclear axis in BaF. All values are shown in atomic units.

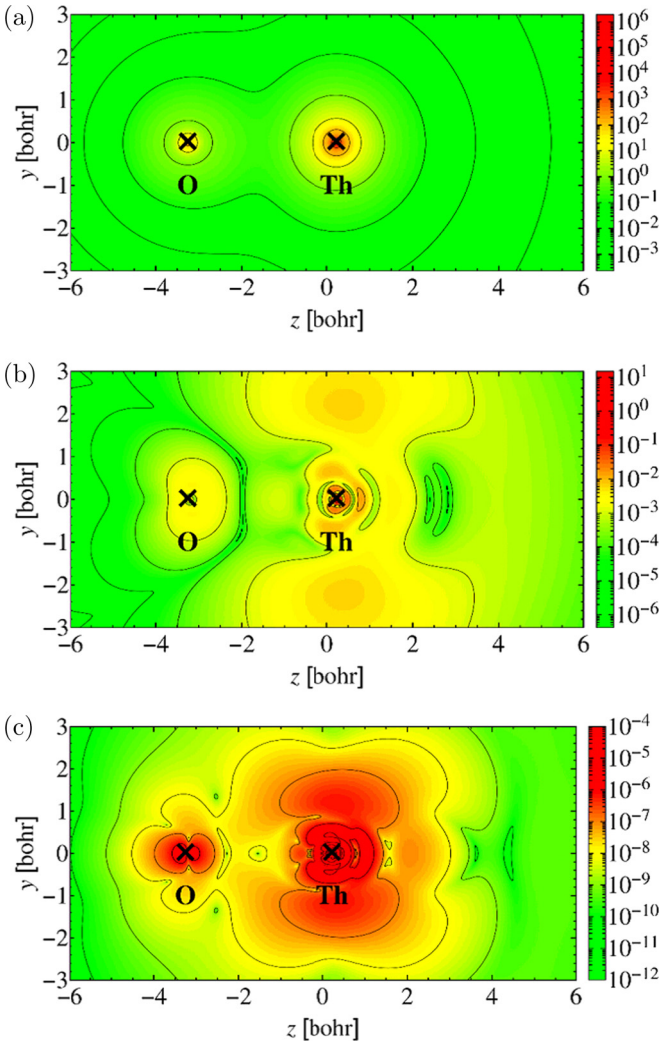

FIG. 4. The distributions of (a) the electron density, (b) the norm of the spin angular momentum density, and (c) the norm of the small component of the spin angular momentum density on a plane including the internuclear axis in ThO. All values are shown in atomic units.

Let us now investigate the distribution of local physical quantities defined by the quantum field theory. The distributions of local physical quantities on a plane including the internuclear axis in YbF, BaF, ThO, and HF^+ are shown in Figs. 2–5, respectively. Panels (a)–(c) in these figures show, respectively, the results of the electron density, the norm of the spin angular momentum density, and the norm of the small component of the spin angular momentum density $|\langle\hat{\psi}_S^\dagger \frac{\hbar}{2}\vec{\sigma}\hat{\psi}_S\rangle|$, all in atomic units. The electron density distributions of YbF, BaF, and ThO have a very similar pattern. The distribution patterns of the spin angular momentum density are quite different from those of the electron density. The distribution patterns of the spin angular momentum density and its small component contribution of YbF are similar to those of BaF, since both of them are in the same state $^2\Sigma_{1/2}$. A remarkable feature of the spin angular momentum density distribution in YbF is that its distribution is not symmetric for both sides of internuclear axis around nuclei and is concentrated at a little distance away from nuclei. This feature is common with that of YbF, BaF, and ThO, which have the large $\mathcal{E}_{\rm eff}$, while it is not seen in HF^+. In Figs. 6(a) and 7(a), we compare the distribution patterns of the spin angular momentum density in YbF and HF^+, respectively. This feature is highlighted in these figures. However, for the effective electric field, $\langle\hat{\psi}_S^\dagger \frac{\hbar}{2}\vec{\sigma}\hat{\psi}_S\rangle$ is more important than the spin angular momentum density itself. The norm value of $\langle\hat{\psi}_S^\dagger \frac{\hbar}{2}\vec{\sigma}\hat{\psi}_S\rangle$ in HF^+ is as large as that in YbF. Since Eq. (15) indicates that the value of the effective electric field depends on the scalar product of $\hat{\psi}_S^\dagger \frac{\hbar}{2}\vec{\sigma}\hat{\psi}_S$ and $\hat{\vec{E}}^{\rm nuc}$, one may presume that the effective electric field in HF^+ is as large as that of YbF; however, this presumption is seen to be wrong from Table VII. As shown in Figs. 5(c) and 7(b), the distribution pattern of $\langle\hat{\psi}_S^\dagger \frac{\hbar}{2}\vec{\sigma}\hat{\psi}_S\rangle$ in HF^+ is nearly antisymmetric to a plane which intersects orthogonally with the internuclear axis on the F nucleus, while the electric field of a nucleus is distributed almost spherically and the direction is radial from the F nucleus. On the other hand, the distribution pattern in

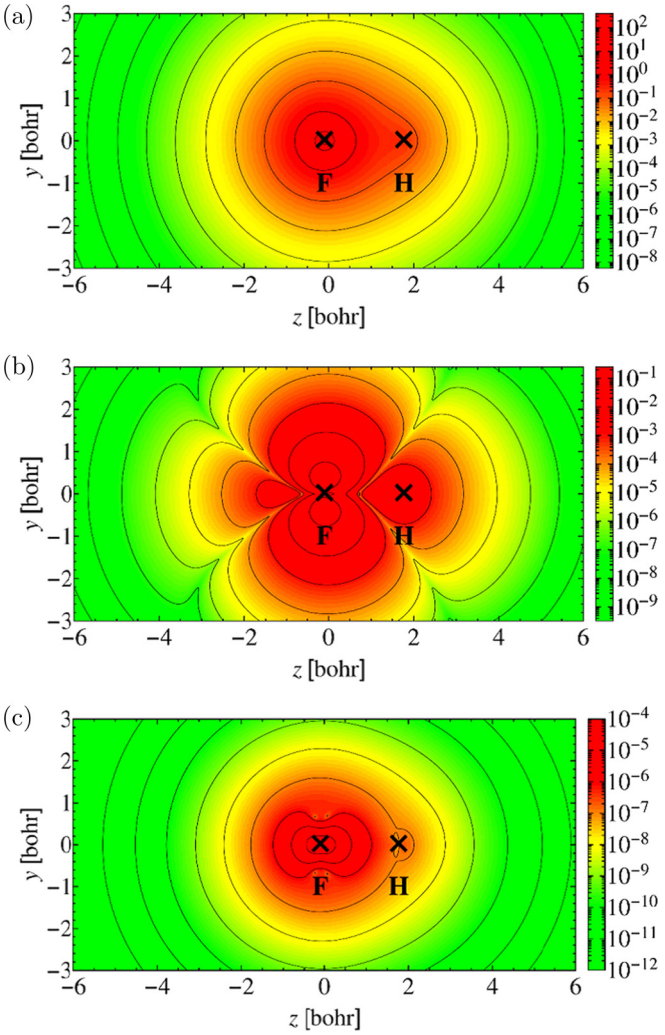

FIG. 5. The distributions of (a) the electron density, (b) the norm of the spin angular momentum density, and (c) the norm of the small component of the spin angular momentum density on a plane including the internuclear axis in HF^+. All values are shown in atomic units.

YbF shown in Fig. 6(b) is asymmetric, though its magnitude of symmetry breaking is smaller than the spin angular momentum density itself. These features can be seen more clearly from the distributions of $\langle \hat{\psi}_S^\dagger \frac{\hbar}{2}\vec{\sigma}\hat{\psi}_S \cdot \hat{\vec{E}}^{\rm nuc}\rangle$ in YbF and HF^+ shown

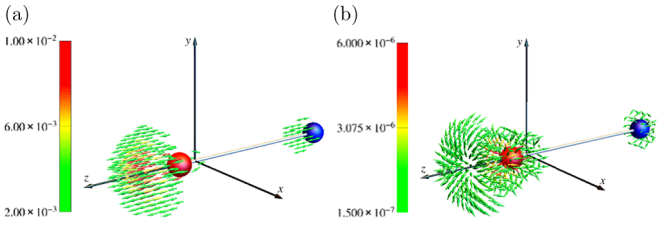

FIG. 6. Distributions of (a) the spin angular momentum density $\langle \hat{\vec{s}}_e\rangle$ and (b) the small component of the spin angular momentum density $\langle \hat{\psi}_S^\dagger \frac{\hbar}{2}\vec{\sigma}\hat{\psi}_S\rangle$ in YbF. The red sphere represents the Yb nucleus and the blue one represents the F nucleus. The color shows the value of densities in atomic units.

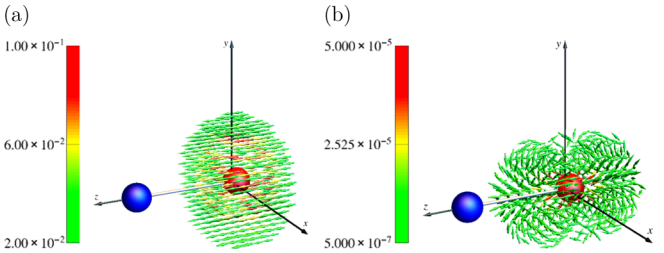

FIG. 7. Distributions of (a) the spin angular momentum density $\langle \hat{\vec{s}}_e\rangle$ and (b) the small component of the spin angular momentum density $\langle \hat{\psi}_S^\dagger \frac{\hbar}{2}\vec{\sigma}\hat{\psi}_S\rangle$ in HF^+. The red sphere represents the F nucleus and the blue one represents the H nucleus. The color shows the value of densities in atomic units.

in Fig. 8. This means that not only the large nucleus charge but also the asymmetric pattern of $|\langle \hat{\psi}_S^\dagger \frac{\hbar}{2}\vec{\sigma}\hat{\psi}_S\rangle|$ are important features of the large effective electric field. As a result, although $|\langle \hat{\psi}_S^\dagger \frac{\hbar}{2}\vec{\sigma}\hat{\psi}_S\rangle|$ in HF^+ is as large as that in YbF, the integration of the inner product of $\hat{\psi}_S^\dagger \vec{\sigma}\hat{\psi}_S$ and $\hat{\vec{E}}^{\rm nuc}$ over the whole region is much smaller than that in YbF. In other words, it can be predicted that even light atomic molecules could have the large effective electric field if the small component of the spin angular momentum density has an asymmetric distribution pattern.

Next, the vector potential term of the spin torque density $\langle \hat{\vec{t}}_{eA}\rangle$ and the EDM torque densities in YbF are shown in Fig. 9. In this article, we adopt atomic units for torque. Among three heavy molecules, we choose YbF for a demonstration, since this molecule is very consistent with other works and is a familiar one due to many works reported by many groups, while the other two molecules have the same features discussed below. The magnetic term of the EDM torque density $\langle \hat{\vec{t}}^{B}_{\rm EDM}\rangle$ is perpendicular to the magnetic field, as seen from Eq. (29), and its distribution is concentrated around the nuclei. On the other hand, the electric term of the EDM torque density $\langle \hat{\vec{t}}^{E}_{\rm EDM}\rangle$ is also perpendicular to the electric field and its distribution pattern is almost the same as that of the spin angular momentum density, where both features are seen from Eq. (28). We also calculate the integration of each torque contribution over the whole region. The value of the vector potential term of the spin torque is $\int \langle \hat{\vec{t}}_{eA}\rangle d^3\vec{r} \approx (0.0, -1.8\times10^{-3}, 0.0)$, which is perpendicular to both magnetic field and spin angular momentum. The integrated value of the electric term of EDM

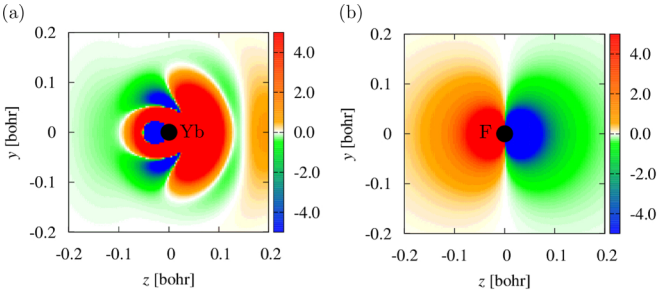

FIG. 8. The distributions of $\langle \hat{\psi}_S^\dagger \frac{\hbar}{2}\vec{\sigma}\hat{\psi}_S \cdot \hat{\vec{E}}^{\rm nuc}\rangle$ in (a) YbF around the Yb nucleus and (b) HF^+ around the F nucleus (in atomic units).

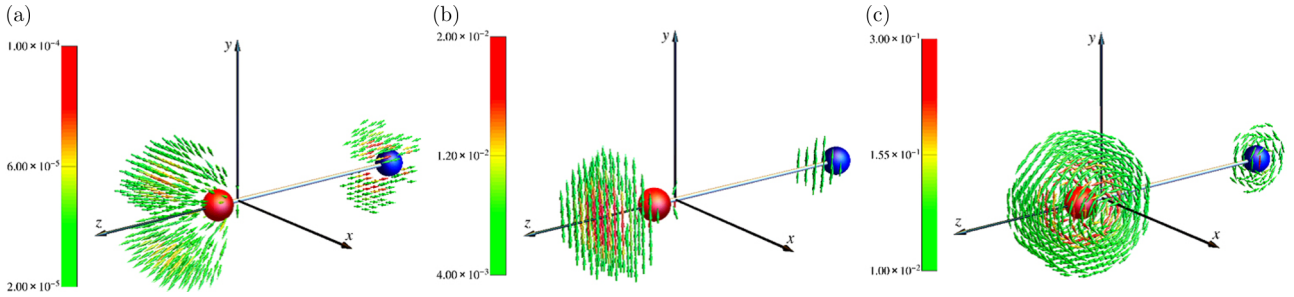

FIG. 9. Distributions of (a) the vector potential term of the spin torque density $\langle \hat{\vec{t}}_{eA} \rangle$, (b) the electric term of the EDM torque density $\langle \hat{\vec{t}}^{E}_{\mathrm{EDM}} \rangle$, and (c) the magnetic term of the EDM torque density $\langle \hat{\vec{t}}^{B}_{\mathrm{EDM}} \rangle$ in YbF. The red sphere represents the Yb nucleus and the blue one represents the F nucleus. The color shows the value of the torque in atomic units.

torque density is $(0.0, 1.0 \times d_e, 0.0)$, which is much larger than that of the magnetic term, $(0.0, 7.3 \times 10^{-6} \times d_e, 0.0)$. This difference between their integrated values can be explained by the difference of their distribution patterns. Since the distribution of $\langle \hat{\vec{t}}^{B}_{\mathrm{EDM}} \rangle$ forms vortices around the nuclei, $\int \langle \hat{\vec{t}}^{B}_{\mathrm{EDM}} \rangle d^3\vec{r}$ is averaged out drastically.

These results confirm that the equation of motion of spin [Eq. (30)] based on the quantum field theory enables us to estimate the integrated value and even to visualize the local pictures of spin torque dynamics, which give us a different perspective of local spin dynamics.

V. CONCLUSIONS

In this paper, we have studied the spin dynamics of the electron from the viewpoint of the electron EDM in the framework of the quantum field theory. The relation between the interaction energy of the electron EDM and the spin precession is described approximately by time evolution originated from the existence of the EDM. We have calculated $\mathcal{E}_{\mathrm{eff}}$ for YbF ($^2\Sigma_{1/2}$), BaF ($^2\Sigma_{1/2}$), ThO ($^3\Delta_1$), and HF^+ ($^2\Pi_{1/2}$) by CI computations based on RASCI. From the viewpoint of the local spin torque dynamics, the modification of the equation of motion of the spin angular momentum density has been discussed and we have shown the spin angular momentum density and the EDM torque density for the above molecules. We have demonstrated that the local pictures of the spin and torque help us to understand some of the physical origin of spin phenomena. We have predicted that even light atomic molecules could have the large effective electric field if the small component of the spin angular momentum density has an asymmetric distribution pattern. In a future work, we will investigate the distribution of the local physical quantities for other molecules and explore new prediction methods of the spin precession. We also study the relation between the local distributions of the torque for the spin and the internal electric field, which is used for experiments in the search for the electron EDM.

ACKNOWLEDGMENTS

This work was supported by a Grant-in-Aid for Scientific Research (Grant No. 25410012), a Grant-in-Aid for JSPS Fellows (Grant No. 14J02866), and by Toyota Physical and Chemical Research Institute Scholars.

[1] For example, see M. Drees, R. M. Godbole, and P. Roy, *Theory and Phenomenology of Particles* (World Scientific, Singapore, 2004).
[2] J. Hisano, M. Nagai, T. Naganawa, and M. Senami, Phys. Lett. B **644**, 256 (2007).
[3] The ACME Collaboration *et al.*, Science **343**, 269 (2014).
[4] J. J. Hudson *et al.*, Nature (London) **473**, 493 (2011); D. M. Kara *et al.*, New J. Phys. **14**, 103051 (2012).
[5] H. M. Quiney *et al.*, J. Phys. B **31**, L85 (1998).
[6] M. Abe, G. Gopakumar, M. Hada, B. P. Das, H. Tatewaki, and D. Mukherjee, Phys. Rev. A **90**, 022501 (2014).
[7] M. K. Nayak and R. K. Chaudhuri, J. Phys. B **39**, 1231 (2006).
[8] T. Fleig and M. K. Nayak, J. Mol. Spectrosc. **300**, 16 (2014).
[9] A. Tachibana, J. Mol. Model **11**, 301 (2005).
[10] M. Senami, J. Nishikawa, T. Hara, and A. Tachibana, J. Phys. Soc. Jpn. **79**, 084302 (2010).
[11] T. Hara, M. Senami, and A. Tachibana, Phys. Lett. A **376**, 1434 (2012).
[12] M. Fukuda, M. Senami, and A. Tachibana, *Advances in Quantum Methods and Applications in Chemistry, Physics, and Biology* Progress in Theoretical Chemistry and Physics, Vol. 27, edited by M. Hotokka, E. J. Brändas, J. Maruani, and G. Delgado-Barrio (Springer, New York, 2013), Chap. 7, pp. 131–139.
[13] L. Schiff, Phys. Rev. **132**, 2194 (1963).
[14] B. P. Das, in *Aspects of Many-Body Effects in Molecules and Extended Systems*, edited by D. Mukherjee (Springer, Berlin, 1989), p. 411.
[15] A. Tachibana, J. Mol. Struct. (THEOCHEM) **943**, 138 (2010).
[16] For example, see A. Messiah, *Quantum Mechanics* (North-Holland, New York, 1961).
[17] A. Tachibana, J. Math. Chem. **50**, 669 (2012).
[18] A. Tachibana, in *Concepts and Methods in Modern Theoretical Chemistry*, edited by S. K. Ghosh and P. K. Chattaraj (CRC, Boca Raton, FL, 2013), pp. 235–251.
[19] A. Tachibana, J. Comput. Chem. Jpn. **13**, 18 (2014).

[20] A. Tachibana, Indian J. Chem. A **53**, 1031 (2014).
[21] A. Tachibana, J. Math. Chem. **53**, 1943 (2015).
[22] L. Visscher, H. J. Aa. Jensen, R. Bast, and T. Saue, with contributions from V. Bakken, K. G. Dyall, S. Dubillard, U. Ekström, E. Eliav, T. Enevoldsen, E. Faßhauer, T. Fleig, O. Fossgaard, A. S. P. Gomes, T. Helgaker, J. K. Lærdahl, Y. S. Lee, J. Henriksson, M. Iliaš, Ch. R. Jacob, S. Knecht, S. Komorovský, O. Kullie, C. V. Larsen, H. S. Nataraj, P. Norman, G. Olejniczak, J. Olsen, Y. C. Park, J. K. Pedersen, M. Pernpointner, K. Ruud, P. Sałek, B. Schimmelpfennig, J. Sikkema, A. J. Thorvaldsen, J. Thyssen, J. van Stralen, S. Villaume, O. Visser, T. Winther, and S. Yamamoto, computer code DIRAC13, a relativistic *ab initio* electronic structure program (2013), see http://www.diracprogram.org.
[23] K. G. Dyall, Theor. Chem. Acc. **117**, 491 (2007); J. Phys. Chem. A **113**, 12638 (2009); A. S. P. Gomes, K. G. Dyall, and L. Visscher, Theor. Chem. Acc. **127**, 369 (2010); K. G. Dyall, *ibid.* **131**, 1217 (2012).
[24] K. G. Dyall, J. Phys. B **31**, 1409 (1998).
[25] N. J. Stone, At. Data Nucl. Data Tables **90**, 75 (2005).
[26] M. Senami, K. Ichikawa, and A. Tachibana, computer code QEDynamics, http://www.tachibana.kues.kyoto-u.ac.jp/qed/ (unpublished).
[27] R. J. Van Zee, M. L. Seely, T. C. DeVore, and W. Weltner, Jr., J. Phys. Chem. **82**, 1192 (1978).
[28] B. E. Sauer, J. Wang, and E. A. Hinds, J. Chem. Phys. **105**, 7412 (1996).
[29] N. S. Mosyagin, M. G. Kozlov, and A. V. Titov, J. Phys. B **31**, L763 (1998).
[30] M. K. Nayak and R. K. Chaudhuri, Pramana **73**, 581 (2009).
[31] W. E. Ernst, J. Kändler, and T. Törring, J. Chem. Phys. **80**, 2283 (1984).
[32] L. B. Knight, Jr., W. C. Easley, W. Weltner, Jr., and M. Wilson, J. Chem. Phys. **41**, 2836 (1964).
[33] M. G. Kozlov, A. V. Titov, N. S. Mosyagin, and P. V. Souchko, Phys. Rev. A **56**, R3326(R) (1997).
[34] P. Hess, Ph.D. thesis, Harvard University, 2014; see http://laserstorm.harvard.edu/edm//publications.html.
[35] L. V. Skripnikov and A. V. Titov, J. Chem. Phys. **142**, 024301 (2015).